Journal of Materials Chemistry A

Accepted Manuscript

This article can be cited before page numbers have been issued, to do this please use: H. Zhang, H. Jiang, Y. Hu, Y. Li, Q. Xu, P. Saha and C. Li, *J. Mater. Chem. A*, 2019, DOI: 10.1039/C9TA00646J.

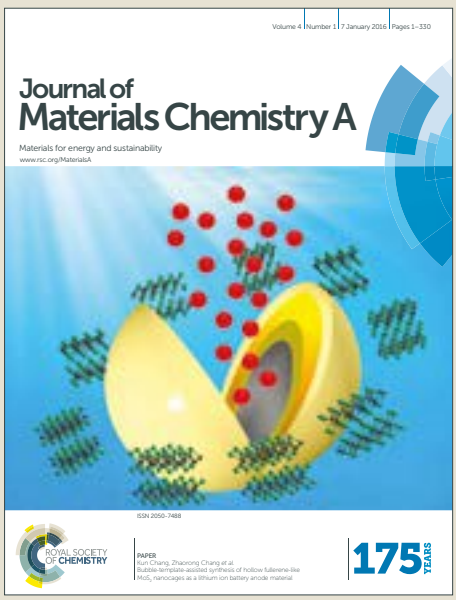

ROYAL SOCIETY OF CHEMISTRY

rsc.li/materials-a

ROYAL SOCIETY OF CHEMISTRY View Article Online
DOI: 10.1039/C9TA00646J

Journal Name

ARTICLE

Tailorable Surface Sulfur Chemistry of Mesoporous Ni_3S_2 Particles for Efficient Oxygen Evolution

Haoxuan Zhang,[a] Hao Jiang,*[a] Yanjie Hu,[a] Yuhang Li,[a] Qiucheng Xu,[a] Saha Petr,[b] Chunzhong Li *[a]

Received 00th January 20xx,
Accepted 00th January 20xx

DOI: 10.1039/x0xx00000x

www.rsc.org/

Boosting intrinsic activity of electrocatalysts is the most pivotal in enhancing oxygen evolution reaction (OER) at the source. Herein, we identify a mesoporous Ni_3S_2 particle electrocatalyst on Ni foam that has appropriate surface sulfur chemistry and demonstrates excellent catalytic activity as well as rapid reaction kinetics. The optimized Ni_3S_2 electrocatalyst shows ultralow overpotentials of 213 and 283 mV at 10 and 100 mA cm^{-2}, respectively, with a very low Tafel slope of 45 mV dec^{-1} in alkaline media. The ECSA normalized current density is 1.1 mA cm^{-2} at the overpotential of 270 mV, nearly three times higher than the pristine Ni_3S_2 (0.4 mA cm^{-2}). It has been observed that sulfur-engineered Ni_3S_2 electrocatalyst can promote more Ni^{3+} generation with significant shift of Ni center binding energy compared with the pristine Ni_3S_2 during OER. The findings propose a facile tactic to improve the intrinsic OER activity for water splitting by optimizing the surface sulfur chemistry of metal sulfide-based electrocatalysts.

Introduction

Oxygen evolution reaction (OER) is the core half reaction of electrochemical water splitting, nitrogen fixation and CO_2 reduction, involving in a complex four electrons transfer step.[1-4] The sluggish kinetics engenders high overpotential (η) for OER, which directly deteriorates the energy conversion efficiency.[5-7] The noble metal (e.g. Ru, Ir) based electrocatalysts have been widely applied to decrease the OER overpotential. However, they are expensive and have limited oxygen evolution activity (η_{10} > 270 mV).[8,9] Therefore, developing efficient and cost-effective electrocatalysts is of great importance. It is well-accepted that the metal bond-containing compounds such as Ni_3S_2 can not only facilitate the adsorption of key catalytic intermediates in alkaline media, but also accelerate charge transfer during OER. They have been considered as a kind of very important electrocatalysts.[10-14] Nevertheless, the overpotential is generally over 300 mV for achieving a current density of 100 mA cm^{-2} because the OER kinetics is significantly decreased under a high current density.[15,16]

To boost the OER kinetics, the main protocols are to increase the number of active sites and enhance the catalytic ability of each active center.[17-19] Among them, the intrinsic activity of electrocatalysts directly determines the OER performance. It has been demonstrated that the intrinsic activity can be significantly enhanced by controlling the surface chemistry state of electrocatalysts and tuning the electron structure of the metal center.[20,21] It is reported that the heterogeneous elements triggered surface chemistry and engineering of electrocatalysts can adjust the adsorption ability to the targeted intermediates and expose more active sites, therefore significantly improving OER performance in alkaline media.[22-24] However, the doping process of non-metal elements (e.g. N, S and P) usually involves a high temperature treatment, which easily causes partial volatilization of these elements. This will have a very limited impact on the active center, impeding the further improvement of the Ni_3S_2 OER performance.

Herein, we demonstrate the synthesis of mesoporous Ni_3S_2 particles on Ni foam by a low temperature hydrothermal route. The surface sulfur chemistry state can be well-tuned by the fine adjustment of reaction temperature. The electronic structure analysis indicates that the surface sulfur dissolution of sulfur-engineered Ni_3S_2 (S-Ni_3S_2) can generate more Ni^{3+} and effectively regulate the electron binding energy of Ni center during OER compared with the pristine Ni_3S_2 and the oxygen-engineered Ni_3S_2 (O-Ni_3S_2). The intrinsic activity is therefore enhanced, markedly boosting OER performance. The S-Ni_3S_2 electrocatalyst only requires an ultralow overpotential of 213 mV at 10 mA cm^{-2} with a very low Tafel slope of 45 mV dec^{-1}. The overpotential is 283 mV when the current density increases to 100 mA cm^{-2}, much smaller than the pristine Ni_3S_2 (341 mV) and the O-Ni_3S_2 (372 mV). This finding realized the rapid and precise regulation of the surface chemistry state of electrocatalysts, giving an avenue for improving the activity of non-noble electrocatalysts.

Results and discussion

[a] Key Laboratory for Ultrafine Materials of Ministry of Education, Shanghai Engineering Research Center of Hierarchical Nanomaterials, School of Materials Science and Engineering & East China University of Science and Technology, Shanghai 200237, China
E-mail: jianghao@ecust.edu.cn (H. Jiang), czli@ecust.edu.cn (C. Z. Li)
[b] Centre of Polymer Systems, University Institute, Tomas Bata University in Zlin, Trida T. Bati 5678, 760 01 Zlin, Czech Republic

Electronic Supplementary Information (ESI) available: details of any supplementary information available should be included here]. See DOI: 10.1039/x0xx00000x

The sulfur-engineered Ni_3S_2 electrocatalyst has been synthesized by a low temperature hydrothermal route, in which L-cysteine as sulfur precursor was directly reacted with Ni foam in aqueous solution at 160 °C for 2 h (see details in Experimental Section). The surface sulfur chemistry state can be well-regulated by the fine adjustment of hydrothermal temperature while other experimental parameters keep unchanged. For comparison, the pristine Ni_3S_2 and O-Ni_3S_2 electrocatalysts have been synthesized at 165 °C and 170 °C, respectively. Typical scanning electron microscopy (SEM) images in **Fig. S1** present similar particle morphology on Ni foam surface for these three samples. Moreover, the transmission electron microscopy (TEM) technique is employed to investigate the microstructure of S-Ni_3S_2 sample, which has an average particle size of about 200 nm (**Fig. 1a**). Furthermore, the corresponding selected area electron diffraction (SAED) pattern indicates the polycrystalline nature of the as-prepared electrocatalyst, which can be indexed to (003) and (300) facets of Ni_3S_2. An enlarged TEM image in **Fig. 1b** shows that the resultant Ni_3S_2 particles are composed of small nanocrystals (6-8 nm) with rich mesoporous arrangement. This is also verified by nitrogen adsorption-desorption isotherms and the corresponding pore-size distribution (**Fig. S2**). The mesoporous feature is benefit to improve catalytic performance by exposing more active sites. The lattice fringe is detected with an inter-planar distance of 0.18 nm relative to Ni_3S_2 (113) facet in the high-resolution TEM image (**Fig. 1c**). In addition, X-ray diffraction (XRD) is applied to characterize the crystallographic structure of the resulting S-Ni_3S_2 particles. As shown in **Fig. 1d**, all diffractive peaks can be indexed to the standard pattern of the rhombohedral Ni_3S_2 phase (JCDPS No. 08-0126) except for three peaks ascribed to metallic Ni substrate, which is in accordance with TEM observation. Meanwhile, the XRD patterns of pristine Ni_3S_2 and

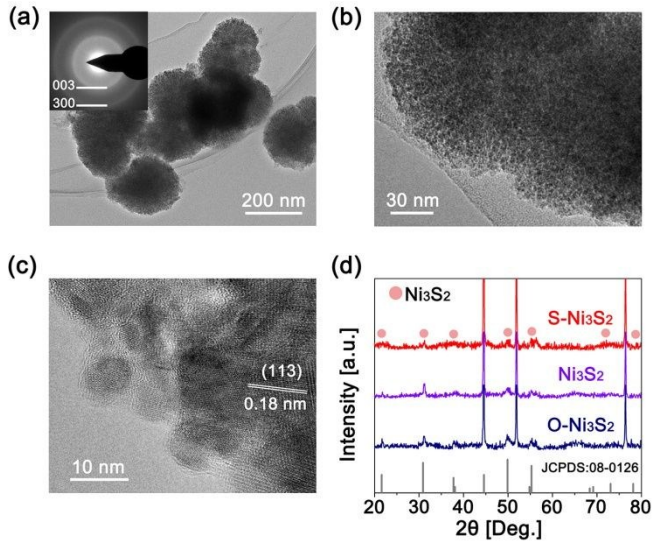

Fig. 1 (a) Low-magnification (*inset* showing the corresponding SAED pattern), (b) high-magnification and (c) high-resolution TEM images of the S-Ni_3S_2 electrocatalysts; (d) XRD patterns of the S-Ni_3S_2, the pristine Ni_3S_2 and the O-Ni_3S_2.

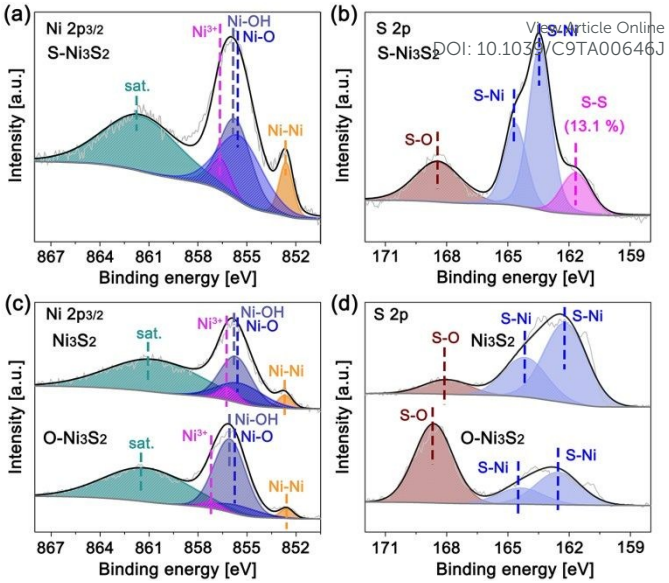

Fig. 2 XPS spectra of Ni $2p_{3/2}$ and S 2p regions of (a, b) the S-Ni_3S_2, (c, d) the pristine Ni_3S_2 and the O-Ni_3S_2.

O-Ni_3S_2 show similar characteristic peaks with those of S-Ni_3S_2, verifying all products are rhombohedral Ni_3S_2 on Ni foam.

The surface chemical state and composition of the S-Ni_3S_2 particles were analyzed by X-ray photoelectron spectroscopy (XPS). The Ni $2p_{3/2}$ region (**Fig. 2a**) can be deconvolved into four characteristic peaks at 852.6, 855.7, 855.8 and 856.7 eV corresponding to Ni-Ni, Ni-O, Ni-OH and Ni^{3+}, respectively, and a satellite peak at 861.9 eV.[25,26] From the S 2p region in **Fig. 2b**, a prominent peak at 161.7 eV with a high content of 13.1 % is attributed to S-S, indicating sulfur elements are well-decorated on the surface.[27] Another two peaks at 163.4 and 164.6 eV can be assigned to S-Ni, whereas the peak at 168.5 eV belongs to S-O owing to the oxidation in air.[28] These results validate the synthesis of S-Ni_3S_2 electrocatalysts. In addition, the high-resolution XPS spectra of pristine Ni_3S_2 and O-Ni_3S_2 particles were also compared in **Fig. 2c**. For Ni $2p_{3/2}$ region, the two samples show different binding energy for the characteristic peaks of Ni-Ni, Ni-O, Ni-OH and Ni^{3+}, indicating the electron structure variation of Ni center. For S 2p regions (**Fig. 2d**), the pristine Ni_3S_2 prepared at 165 °C has the similar position and intensity of S-Ni and S-O peaks with previous literatures.[29,30] In contrast, the sample prepared at 170 °C gives the significantly enhanced intensity of S-O peak, implying oxygen elements are bonded on the surface to form O-Ni_3S_2. Based on above results, it is verified that the fine adjustment of reaction temperature can effectively tune the surface sulfur chemistry state of Ni_3S_2 to regulate the electronic structure of Ni center, which is critical for improving OER performances.

The OER performances of S-Ni_3S_2 electrocatalyst are evaluated with pristine Ni_3S_2, O-Ni_3S_2 and commercial benchmark RuO_2 electrocatalysts as controls in a standard three-electrode system containing 1.0 M KOH (see details in Experimental Section). Linear sweep voltammetry is

View Article Online
DOI: 10.1039/C9TA00646J

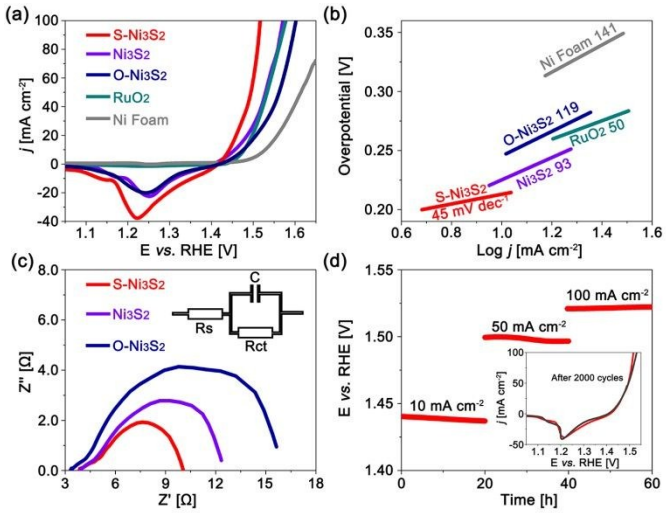

Fig. 3 (a) OER polarization curves in O_2-saturated 1.0 M KOH, (b) Tafel plots and (c) Nyquist plots of the S-Ni_3S_2, the pristine Ni_3S_2 and the O-Ni_3S_2; (d) chronopotentiometry response of the S-Ni_3S_2 electrocatalysts at 10, 50 and 100 mA cm^{-2}, respectively (*inset* showing OER polarization curves after 2000 cycles).

performed at a slow scan rate of 1 mV s^{-1} to attain OER polarization curves with minimal capacitive current. As illustrated in **Fig. 3a**, the S-Ni_3S_2 electrocatalyst requires ultralow overpotentials of 213 and 286 mV to achieve the current densities of 10 and 100 mA cm^{-2}, respectively, which are much lower than those of pristine Ni_3S_2 (η_{10}=226, η_{100}=341 mV), O-Ni_3S_2 (η_{10}=247, η_{100}=372 mV) and commercial RuO_2 (η_{10}=249, η_{100}=342 mV). This is also confirmed by the cyclic voltammetry (CV) curve in **Fig. S3**. Such remarkable performances are comparable to most of reported Ni_3S_2-based electrocatalysts to date (**Table S1**). The Tafel slope is a commonly representative indicator to assess reaction kinetics of electrocatalyst, which can reflect the change rate of current density with increase of overpotentials. Thus, the small Tafel slope of S-Ni_3S_2 (45 mV dec^{-1}), that superior to those of pristine Ni_3S_2 (93 mV dec^{-1}), O-Ni_3S_2 (119 mV dec^{-1}) and commercial benchmark RuO_2 (50 mV dec^{-1}) (**Fig. 3b**), suggests the accelerated OER kinetics caused by surface sulfur engineering. Further assessment of the reaction kinetics is applied by the electrochemical impedance spectroscopy (EIS) measurement. **Fig. 3c** is the corresponding Nyquist plots, in which the high- and low-frequency responses can be attributed to the solution resistance (R_s) and interfacial charge-transfer resistance (R_{ct}) during OER, respectively. Notably, the R_{ct} of S-Ni_3S_2 catalyst is much smaller than other controls, thus confirming the boosted OER kinetics.

Catalytic stability is also a crucial evaluation for catalytic performances. The chronopotentiometric measurement (CP) is thus carried out in O_2-saturated 1.0 M KOH, showing negligible potential drop for the S-Ni_3S_2 electrocatalysts even after sustaining at 10, 50 and 100 mA cm^{-2} for 60 h, as shown in **Fig. 3d**. The stability is also evidenced by the comparison of OER polarization curves before and after 2000 cycles (*inset* of **Fig. 3d**). In addition, the XRD pattern of S-Ni_3S_2 sample after 60 h OER test (**Fig. S4**) exhibits unchanged diffractive peaks, further verifying the outstanding OER stability. The surface sulfur engineering can accelerate reaction kinetics to reduce overpotentials, and meanwhile stabilize OER process with slight potentials change even after long-term test.

To shed light on the effect of surface sulfur engineering on improving OER performances, the intrinsic performances of the S-Ni_3S_2, pristine Ni_3S_2 and O-Ni_3S_2 electrocatalysts are systematically studied. The electrochemically active surface areas (ECSA) are firstly calculated according to the double-layer specific capacitances (**Fig. S5 & Fig. S6**), which show a much higher value of 12.3 cm^2 for the S-Ni_3S_2 in comparison to those of the pristine Ni_3S_2 (8.4 cm^2) and the O-Ni_3S_2 (2.9 cm^2), indicating sulfur engineering is helpful to the exposure of active sites (**Fig. 4a**).[31,32] Subsequently, the ECSA values are applied to estimate the specific current densities (**Fig. 4b**), exhibiting the highest current density of 1.1 mA cm^{-2} at the overpotential of 270 mV for S-Ni_3S_2 electrocatalyst, almost three times higher than the pristine Ni_3S_2 (0.4 mA cm^{-2}).[33] Similar trends are also obtained from the mass activities calculated by the Ni content on the surface (**Fig. S7**).[34] The current density of 4.4 A g^{-1} for S-Ni_3S_2 is achieved at the same overpotential (**Fig. 4c**), which is approximately 2.4 and 3.7 times higher than the pristine Ni_3S_2 (1.8 A g^{-1}) and the O-Ni_3S_2 (1.3 A g^{-1}). Turnover frequencies (TOFs) are further calculated by integrating the Ni redox feature from the OER polarization curves.[35] In **Fig. 4d**, a high TOF value of 8 × 10^{-4} s^{-1} of the S-Ni_3S_2 sample is 2.7 and 4.0 times higher than those of the pristine Ni_3S_2 (3 × 10^{-4} s^{-1}) and the O-Ni_3S_2 (2 × 10^{-4} s^{-1}). As a result, the key feature of sulfur engineering on the surface of Ni_3S_2 is to enhance the intrinsic activities for markedly boosting OER performances in alkaline media.

To gain in-depth insight into the enhanced intrinsic activity caused by surface sulfur engineering, the chemical state variation of S-Ni_3S_2 catalyst after different reaction time is investigated using high-resolution XPS spectra. **Fig. 5a** presents the Ni $2p_{3/2}$ region of S-Ni_3S_2 sample before and after OER.

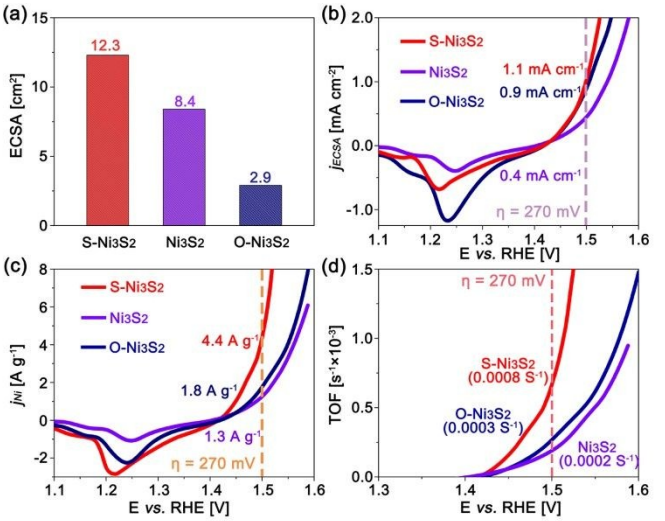

Fig. 4 (a) Electrochemically active surface areas of the S-Ni_3S_2, the pristine Ni_3S_2 and the O-Ni_3S_2; (b) ECSA-normalized and (c) mass-normalized OER polarization curves, and (d) turnover frequency curves of the S-Ni_3S_2, the pristine Ni_3S_2 and the O-Ni_3S_2.

View Article Online
DOI: 10.1039/C9TA00646J

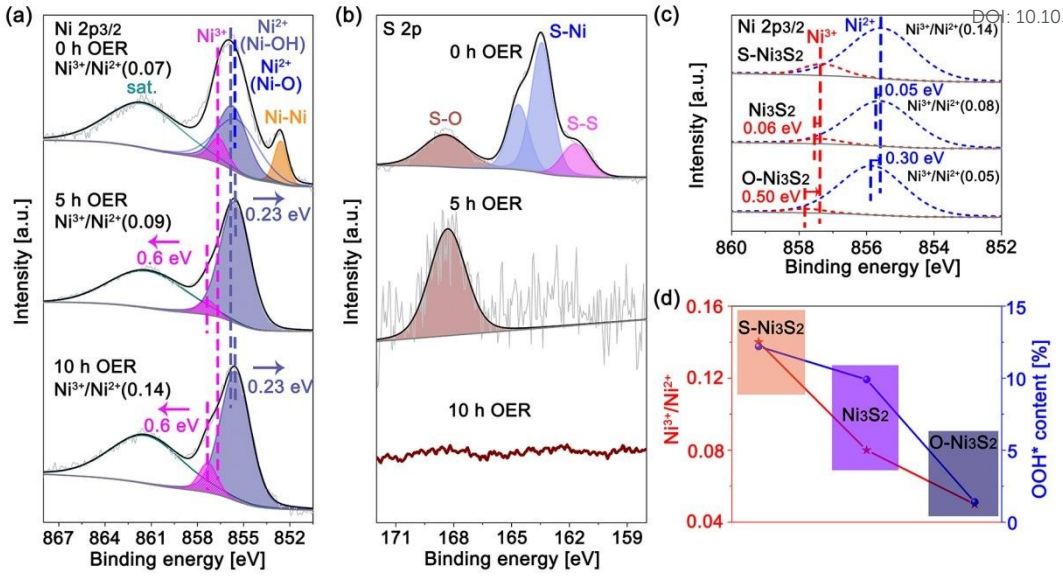

Fig. 5 XPS spectra of (a) Ni $2p_{3/2}$ and (b) S 2p regions of the S-Ni_3S_2 electrocatalysts after 0, 5 and 10 h OER at 20 mA cm^{-2} in O_2-saturated 1.0 KOH, respectively; (c) comparison of XPS spectra of Ni $2p_{3/2}$ region after 10 h and (d) relationship of Ni^{3+}/Ni^{2+} ratio and OOH* content for the S-Ni_3S_2, the pristine Ni_3S_2 and the O-Ni_3S_2.

When the reaction time is 5 h, the characteristic peak of Ni-OH is improved with the disappearance of the Ni-O and Ni-Ni peaks, revealing the initial adsorption of OH* intermediates at electrode-electrolyte interface to convert both Ni-O and Ni-Ni into Ni-OH.[36,37] The Ni^{3+}/Ni^{2+} ratio calculated by integrating peak areas is increased to 0.09, indicating more Ni^{3+} generation during OER. Moreover, a significant positive binding energy shift of 0.6 eV can be calculated for Ni^{3+} while a negative shift of 0.23 eV for Ni-OH. When the reaction time is prolonged to 10 h, the Ni^{3+}/Ni^{2+} ratio is further increased to 0.14 with the unchanged binding energy, indicating the surface of S-Ni_3S_2 has been in the stable chemical state with maximum Ni^{3+} content. The corresponding S 2p region (**Fig. 5b)** shows that the S-S and S-Ni peaks are vanished after 10 h OER, implying the entire dissolution of the sulfur on the surface during reaction process. The intriguing phenomena reveal that the surface sulfur dissolution of S-Ni_3S_2 effectively regulates the electron structure of Ni center. Furthermore, the Ni $2p_{3/2}$ region of the S-Ni_3S_2, the pristine Ni_3S_2 and the O-Ni_3S_2 are compared (**Fig. 5c**). It can be seen that the S-Ni_3S_2 have the highest Ni^{3+}/Ni^{2+} ratio and negative locations of binding energy for Ni^{2+} and Ni^{3+}, which can promote the adsorption ability of Ni center to key active intermediates (OOH*) in OER.[38,39] The relationship of Ni^{3+}/Ni^{2+} ratio and OOH* content for these three samples is provided in **Fig. 5d**, displaying that the Ni^{3+}/Ni^{2+} ratio is in direct proportion to OOH* content. Obviously, the S-Ni_3S_2 electrocatalysts give the highest OOH* content of 12.2 % (**Fig. S8**), which is in accordance with the above analysis. Therefore, surface sulfur engineering can facilitate more Ni^{3+} generation with significant shift of Ni center binding energy, thus enhancing the intrinsic activity to markedly boost OER performance.

Conclusions

In summary, a mesoporous Ni_3S_2 particle electrocatalyst on Ni foam has been synthesized by a low temperature hydrothermal route. The surface sulfur chemistry state can be effectively tuned by finely adjusting reaction temperature. The S-Ni_3S_2 electrocatalysts only require an ultralow overpotential of 213 mV at 10 mA cm^{-2} with a very low Tafel slope of 45 mV dec^{-1}. Even at a higher current density of 100 mA cm^{-2}, the overpotential is still 283 mV, much lower than the pristine Ni_3S_2 (341 mV) and the O-Ni_3S_2 (372 mV). Such impressive performances surpass benchmark RuO_2 and most reported Ni_3S_2-based electrocatalysts to date. Based on electronic structure analysis, it is discovered that the surface sulfur dissolution can promote more Ni^{3+} generation and effectively regulate the binding energy of Ni center during OER in comparison with the pristine Ni_3S_2 and the O-Ni_3S_2, thus enhancing intrinsic activity to markedly boost OER performance. The facile tactic for rapidly and precisely regulating the surface chemistry state of electrocatalysts can be applied to other materials towards efficient oxygen generation.

Conflicts of interest

There are no conflicts to declare.

Acknowledgements

This work was supported by the National Natural Science Foundation of China (21838003, 21808061 and 91534122), the Social Development Program of Shanghai (17DZ1200900), the

Shanghai Scientific and Technological Innovation Project (18JC1410600 and 18DZ2252400), the Program for Professor of Special Appointment (Eastern Scholar) at Shanghai Institutions of Higher Learning, and the Fundamental Research Funds for the Central Universities (222201718002).

References

1. Z. W. Seh, J. Kibsgaard, C. F. Dickens, I. Chorkendorff, J. K. Nørskov and T. F. Jaramillo, *Science*, 2017, **355**, eaad4998.
2. S. Ji, Z. Wang and J. Zhao, *J. Mater. Chem. A*, 2019, DOI: 10.1039/C8TA10497B.
3. C. Hu, L. Zhang, Z. J. Zhao, J. Luo, J. Shi, Z. Huang, J. Gong, *Adv. Mater.*, 2017, **29**, 1701820.
4. X. Shi, H. Wang, P. Kannan, J. Ding, S. Ji, F. Liu, H. Gai and R. Wang, *J. Mater. Chem. A*, 2019, **7**, 3344-3352.
5. H. C. Tao, Y. A. Gao, N. Talreja, F. Guo, J. Texter, C. Yan and Z. Y. Sun, *J. Mater. Chem. A*, 2017, **5**, 7257-7284.
6. B. Zhao, L. Zhang, D. Zhen, S. Yoo, Y. Ding, D. Chen, Y. Chen, Q. Zhang, B. Doyle, X. Xiong and M. Liu, *Nat. Commun.*, 2017, **8**, 14586.
7. J. Ding, P. Wang, S. Ji, H. Wang, D. J. L. Brett and R. Wang, *Electrochim. Acta*, 2019, **300**, 93-101.
8. C. Hu, L. Zhang, Z. J. Zhao, A. Li, X. Chang, J. Gong, *Adv. Mater.*, 2018, **12**, 1705538.
9. Y. Lee, J. Suntivich, K. J. May, E. E. Perry, Y. Shao-Horn, *J. Phys. Chem. Lett.*, 2012, **3**, 399-404.
10. W. Zhou, X. J. Wu, X. Cao, X. Huang, C. Tan, J. Tian, H. Liu, J. Wang, H. Zhang, *Energy Environ. Sci.*, 2013, **6**, 2921-2924.
11. G. Zhang, Y. S. Feng, W. T. Lu, D. He, C. Y. Wang, Y. K. Li, X. Y. Wang, F. F. Cao, *ACS Catal.*, 2018, **8**, 5431-5441.
12. J. J. Lv, J. Zhao, H. Fang, L. P. Jiang, L. L. Li, J. Ma, J. J. Zhu, *Small*, 2017, **13**, 1700264.
13. Y. Rao, H. Ning, X. Ma, Y. Liu, Y. Wang, H. Liu, J. L. Liu, Q. S. Zhao, M. B. Wu, *Carbon*, 2018, **129**, 335-341.
14. Q. Xu, H. Jiang, H. Zhang, Y. Hu, C. Li, *Appl. Catal. B: Environ.* 2018, **242**, 60-66.
15. L. Y. Zeng, K. A. Sun, Z. C. Yang, S. L. Xie, Y. J. Chen, Z. Liu, Y. Q. Liu, J. C. Zhao, Y. Q. Liu, C. G. Liu, *J. Mater. Chem. A*, 2018, **6**, 4485-4493.
16. L. L. Feng, G. Yu, Y. Wu, G. D. Li, H. Li, Y. Sun, T. Asefa, W. Chen and X. Zou, *J. Am. Chem. Soc.*, 2015, **137**, 14023-14026.
17. A. S. Batchellor and S. W. Boettcher, *ACS Catal.*, 2015, **5**, 6680-6689.
18. S. H. Zou, M. S. Burke, M. G. Kast, J. Fan, N. Danilovic, S. W. Boettcher, *Chem. Mater.*, 2015, **27**, 8011-8020.
19. L. M. Cao, J. W. Wang, D. C. Zhong and T. B. Lu, *J. Mater. Chem. A*, 2018, **6**, 3224-3230.
20. P. Z. Chen, K. Xu, Z. W. Fang, Y. Tong, J. C. Wu, X. L. Lu, X. Peng, H. Ding, C. Z. Wu, Y. Xie, *Angew. Chem. Int. Edit.*, 2015, **54**, 14710-14714.
21. B. K. Kim, S. K. Kim, S. K. Cho, J. J. Kim, *Appl. Catal. B: Environ.*, 2018, **237**, 409-415.
22. P. Z. Chen, T. P. Zhou, M. X. Zhang, Y. Tong, C. G. Zhong, N. Zhang, L. D. Zhang, C. Z. Wu, Y. Xie, *Adv. Mater.*, 2017, **29**, 1701584.
23. X. Zhang, X. Zhang, H. Xu, Z. Wu, H. Wang, Y. Liang, *Adv. Funct. Mater.*, 2017, **27**, 1606635.
24. Q. Liu, L. S. Xie, Z. Liu, G. Du, A. M. Asiri, X. P. Sun, *Chem. Commun.*, 2017, **53**, 12446-12449.
25. M. C. Biesinger, B. P. Payne, A. P. Grosvenor, L. W. M. Lau, A. R. Gerson, R. S. C. Smart, *Appl. Surf. Sci.*, 2011, **257**, 2717-2730.
26. A. P. Grosvenor, M. C. Biesinger, R. S. C. Smart, N. S. McIntyre, *Surf. Sci.*, 2006, **600**, 1771-1779.
27. H. Vrubel, D. Merki, X. Hu, *Energy Environ. Sci.*, 2012, **5**, 6136-6144.
28. T. Yokoyama, A. Imanishi, S. Terada, H. Namba, Y. Kitajima, T. Ohta, *Surf. Sci.*, 1995, **334**, 88-94.
29. Q. Wang, R. Gao, J. H. Li, *Appl. Phys. Lett.*, 2007, **90**, 143107.
30. P. Hu, T. Wang, J. Zhao, C. Zhang, J. Ma, H. Du, X. Wang, G. Cui, *ACS Appl. Mater. Interfaces*, 2015, **7**, 26396-26399.
31. C. C. L. McCrory, S. Jung, J. C. Peters, T. F. Jaramillo, *J. Am. Chem. Soc.*, 2013, **135**, 16977-16987.
32. Y. Pi, N. Zhang, S. Guo, J. Guo, X. Huang, *Nano Lett.*, 2016, **16**, 4424-4430.
33. Y. Yang, K. Zhang, H. Lin, X. Li, H. C. Chan, L. Yang, Q. Gao, *ACS Catal.*, 2017, **7**, 2357-2366.
34. L. H. Wu, Q. Li, C. H. Wu, H. Y. Zhu, A. Mendoza-Garcia, B. Shen, J. H. Guo, S. H. Sun, *J. Am. Chem. Soc.*, 2015, **137**, 7071-7074.
35. L. Trotochaud, S. L. Young, J. K. Ranney and S. W. Boettcher, *J. Am. Chem. Soc.*, 2014, **136**, 6744-6753.
36. B. Konkena, J. Masa, A. J. R. Botz, I. Sinev, W. Xia, J. Koßmann, R. Drautz, M. Muhler, W. Schuhmann, *ACS Catal.*, 2017, **7**, 229-237.
37. B. Song, K. Li, Y. Yin, T. Wu, L. Dang, M. Cabán-Acevedo, J. Han, T. Gao, X. Wang, Z. Zhang, J. R. Schmidt, P. Xu, S. Jin, *ACS Catal.*, 2017, **7**, 8549-8557.
38. D. Friebel, M. W. Louie, M. Bajdich, K. E. Sanwald, Y. Cai, A. M. Wise, M. J. Cheng, D. Sokaras, T. C. Weng, R. Alonso-Mori, R. C. Davis, J. R. Bargar, J. K. Nørskov, A. Nilsson, A. T. Bell, *J. Am. Chem. Soc.*, 2015, **137**, 1305-1313.
39. H. Zhang, H. Jiang, Y. Hu, P. Saha, C. Li, *Mater. Chem. Front.*, 2018, **2**, 1462-1466.

View Article Online
DOI: 10.1039/C9TA00646J

Journal Name

ARTICLE

The table of contents entry

Tailoring surface sulfur chemistry of Ni_3S_2 can enrich Ni^{3+} and regulate Ni binding energy, thus intrinsically boosting OER performance.

TOC Figure